Biochimica et Biophysica Acta 1851 (2015) 1577–1586

Contents lists available at ScienceDirect

Biochimica et Biophysica Acta

journal homepage: www.elsevier.com/locate/bbalip

Destabilization of the torsioned conformation of a ligand side chain inverts the LXRβ activity

Lautaro D. Álvarez [a,1], M. Virginia Dansey [b,1], Diego Y. Grinman [b], Daniela Navalesi [b], Gisela A. Samaja [a], M. Celeste del Fueyo [a], Niek Bastiaensen [c], René Houtman [c], Darío A. Estrin [d], Adriana S. Veleiro [a], Adali Pecci [b,*], Gerardo Burton [a,*]

[a] Dpto. Química Orgánica and UMYMFOR (CONICET-UBA), Facultad de Ciencias Exactas y Naturales, Universidad de Buenos Aires, Argentina
[b] Dpto. Química Biológica and IFIBYNE (UBA-CONICET), Facultad de Ciencias Exactas y Naturales, Universidad de Buenos Aires, Argentina
[c] Pamgene International BV, 5211HH Den Bosch, The Netherlands
[d] Dpto. Química Inorgánica Analítica y Química Física and INQUIMAE (CONICET-UBA), Facultad de Ciencias Exactas y Naturales, Universidad de Buenos Aires, Argentina

ARTICLE INFO

Article history:
Received 8 May 2015
Received in revised form 11 September 2015
Accepted 24 September 2015
Available online 3 October 2015

Keywords:
Liver X receptors
Inverse agonism
Molecular dynamics
Cholestenoic acid

ABSTRACT

Background: Liver X receptors (LXRs) are transcription factors activated by cholesterol metabolites containing an oxidized side chain. Due to their ability to regulate lipid metabolism and cholesterol transport, they have become attractive pharmacological targets. LXRs are closely related to DAF-12, a nuclear receptor involved in nematode lifespan and regulated by the binding of C-27 steroidal acids. Based on our recent finding that the lack of the C-25 methyl group does not abolish their DAF-12 activity, we evaluated the effect of removing it from the (25R)-cholestenoic acid, a LXR agonist.
Methods: The binding mode and the molecular basis of action of 27-nor-5-cholestenoic acid were evaluated using molecular dynamics simulations. The biological activity was investigated using reporter gene expression assays and determining the expression levels of endogenous target genes. The in vitro MARCoNI assay was used to analyze the interaction with cofactors.
Results: 27-Nor-5-cholestenoic acid behaves as an inverse agonist. This correlates with the capacity of the complex to better bind corepressors rather than coactivators. The C-25 methyl moiety would be necessary for the maintenance of a torsioned conformation of the steroid side chain that stabilizes an active LXRβ state.
Conclusion: We found that a 27-nor analog is able to act as a LXR ligand. Interestingly, this minimal structural change on the steroid triggered a drastic change in the LXR response.
General significance: Results contribute to improve our understanding on the molecular basis of LXRβ mechanisms of action and provide a new scaffold in the quest for selective LXR modulators.

1. Introduction

Nuclear receptors (NRs) constitute a conserved family of ligand-inducible transcription factors, involved in numerous essential processes in living cells. In the last decade, the nuclear liver X receptors (LXRα and LXRβ), have emerged as attractive pharmacological targets due to their ability to regulate lipid metabolism and transport, as well as inflammatory response [1–3]. Many potential applications targeting LXRs have been proposed for the treatment of several diseases such as atherosclerosis, type 2 diabetes and Alzheimer, among others [4,5]. In this context, considerable efforts have been made by both the academy and the pharmaceutical industry to improve their knowledge on the LXR mechanisms of action. Similarly to other class II NRs, LXRs regulate transcription as a heterodimer, together with the retinoid X receptor (RXR) [1]. This complex binds to specific response elements located in LXR target genes regulatory elements [6]. In the absence of ligand, the LXR/RXR complex preferentially recruits nuclear receptor corepressors (i.e. NCoRs), but upon agonist ligand binding corepressors are released concomitantly with the recruitment of coactivators (i.e. NCoAs) and the general transcriptional machinery [4].

The endogenous LXR ligands are cholesterol metabolites that include an oxidized steroid side chain. Among them, the 24S,25-epoxycholesterol (**1**, Chart 1) and specific hydroxylated derivatives are the major LXR systemic ligands [7]. Other steroids containing a carboxylic terminal group, such as hyodesoxycholic acid, a natural C24 bile acid and the 25R-cholestenoic acid (**2**, Chart 1), a C27 metabolite highly present in the

Abbreviations: ABCG1, ATP-binding cassette sub-family G member 1; FASN, Fatty Acid Synthase gene; LBP, Ligand binding pocket; LXR, Liver X receptor; MD, Molecular Dynamics; NR, Nuclear receptor; SREBP-1a/c, Sterol Response Element Binding Protein1 isoforms a and c.

* Corresponding authors.
E-mail addresses: apecci@qb.fcen.uba.ar (A. Pecci), burton@qo.fcen.uba.ar (G. Burton).
[1] Both authors contributed equally to this work.

http://dx.doi.org/10.1016/j.bbalip.2015.09.007
1388-1981/

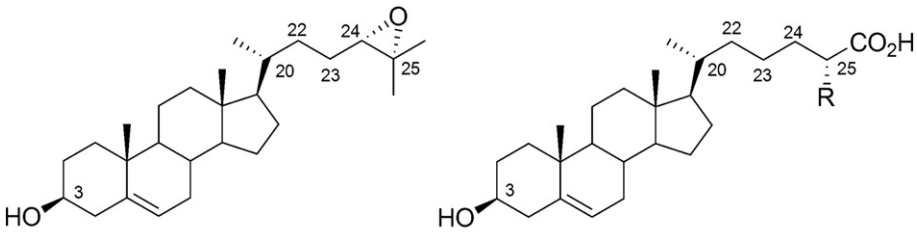

Chart 1. LXR ligands.

lung [8] and in the cerebrospinal fluid [9], have also been described as LXR agonists [5,9,10]. Interestingly, a group of related steroids with a carboxylic group at C-27 (the dafachronic acids, DA) are the main endogenous ligands of a NR (DAF-12) that acts as master regulator of nematode development and lifespan [11]. LXRs were identified, together with the farnesyl X receptor (FXR) and the vitamin D receptor (VDR), as the main human NRs whose protein sequences share high similarity with the *Caenorhabditis elegans* DAF-12 receptor [12]. The fact that similar cholesterol metabolites are able to activate such evolutionary related receptors suggests that a conserved ligand–receptor mechanism may be considered, to investigate structure–activity relationships of LXR ligands. In this context, we have recently shown that removal of the C-25 methyl group did not impede the strong interaction between the C-27 carboxylate of DAs and specific residues of the ligand binding pocket (LBP) of the *ce*DAF-12 receptor [13]. Accordingly, we found that 27-nor-Δ^4-DA retains the DAF-12 agonist activity in both in vitro and in vivo assays [14]. Based on these results, we have now analyzed the effect of the 27-nor analog of **2**, 27-nor-5-cholestenoic acid (**3**, Chart 1) on LXR conformation and activity.

2. Results and discussion

2.1. Ligand binding mode of compound *3* in the LXRβ LBD

We first evaluated the potential of compound **3** to properly recognize specific LBP residues of the LXR, by performing a 150 ns Molecular Dynamics (MD) simulation of the LXRβ/**3** complex. Taking advantage that the LXRβ LBD was crystallized with compound **1** (pdb: 1p8d), we used this structure to construct the initial LXRβ/**3** coordinates. MD simulation of the LXRβ/**1** complex as a control agonist system, showed that the ligand binding mode (depicted in Fig. 1a) is highly conserved during the timescale of the simulation (Figs. 1c, S1a, S1d). Hydrophobic interactions between the steroid skeleton and the non-polar LBP residues maintain the ligand in its original position.

The 3β-hydroxyl group of compound **1** is surrounded by two polar residues, Arg319 and Asn239, while at the other end of the steroid molecule, the epoxy group forms a very strong and stable hydrogen bond with the His435 (Figs. 1a and S1a), consistent with the X ray data [15]. The side chain of compound **1** conserves a torsioned conformation with torsion angles C20–C22–C23–C24 (d_1) and C22–C23–C24–C25 (d_2) fluctuating around 180° and 90°, respectively (Fig. S1d). In the case of compound **3**, the binding mode analysis reveals that the global orientation of this ligand is also conserved along the timescale of simulation (Fig. 1c). However, significant differences exist in the side chain conformation and in the recognition of its polar group. After an initial rearrangement, the C-27 carboxyl group not only interacts with His435, but also forms sporadic hydrogen bonds with the amide side chain of Gln438 (Figs. 1b and S1b). In this conformation, the steroid side chain exhibits more flexibility than that observed with compound **1**, and a fully extended conformation (d_1 and d_2 ca. 180°) turns out to be the most stable (Fig. S1e). In this way, our simulation suggests that compound **3** would have the ability to bind to LXRβ in a similar global mode than compound **1**, but with a different side chain conformation.

2.2. Synthesis and biological activity of compound *3*

In order to evaluate whether compound **3** was actually able to bind to the LXRs, it was synthesized as outlined in Scheme 1 and its biological activity determined by using a luciferase reporter assay in HEK293T cells co-transfected with full length human LXRα or LXRβ.

Cholenaldehyde **4** was prepared from 3α,6α-dihydroxy-5β-cholanic acid following the procedure previously described by us [16]. The 2-carbon homologation was carried out on compound **4** using a Wittig reaction with in situ generation of the stabilized ylide ($[Ph_3PCH_2CO_2Et]Br$, CH_2Cl_2-$NaHCO_3$ (aq)), followed by the regioselective hydrogenation of the side chain double bond. Cleavage of the TBDMS ether with 40% hydrofluoric acid and basic hydrolysis of the C-26 ethyl ester gave compound **3** (48.8% yield from **4**).

The reporter gene assay revealed that, in contrast to compound **2**, compound **3** per se has no effect at 1 μM, but it significantly reduced basal levels of luciferase activity at 10 μM in both LXRα and LXRβ (Fig. 2a). Moreover, when this steroid was co-administered together with the synthetic LXR agonist GW3965, a marked inhibitory effect was observed for both LXRs (Fig. 2b). Taken together, these results indicate that the simplified side chain analog behaves as an LXR inverse agonist. Thus, an apparently small structural change as the removal of the C-25 methyl moiety caused a drastic outcome in the LXR activity profile.

The activity of compound **3** was also evaluated by determining the expression levels of three endogenous LXR target genes, the Fatty Acid Synthase (FASN), the Sterol Response Element Binding Protein1 (SREBP-1a/c) and the ATP-binding cassette sub-family G member 1 (ABCG1) in human hepatic HepG2 cells that express both LXR isoforms. Results depicted in Fig. 2c show that compound **3** per se significantly downregulated the basal expression of FASN and SREBP-1a/c, but did not show any effect on ABCG1 expression. Co-incubation of compound **3** with GW3965 completely blocked GW3965-dependent expression induction of FASN and SREBP-1a/c, however it was unable to inhibit the expression of ABCG1. Furthermore compound **3** did not affect HepG2 cell viability at the assayed concentration (Fig. S2). In the case of compound **2**, an agonist effect on ABCG1 expression was observed, in agreement with the result obtained by Theofilopoulos et al. in SN4741 neuronal cells [17]. Surprisingly, this compound showed no effect on SREBP-1a/c expression and an inverse agonism on FASN. Taken together these results indicate that the effect of these compounds is dependent on the gene analyzed, nevertheless a different activity profile is evident from the above data.

2.3. Molecular basis of action of compound *3*

On the basis of structural data, the molecular mechanism of LXRβ agonist activation has been attributed [15] to an aromatic–aromatic interaction between the His435 (H11) and the Trp457 residue located at the end of H12. The positioning of helix 12 determines the activation

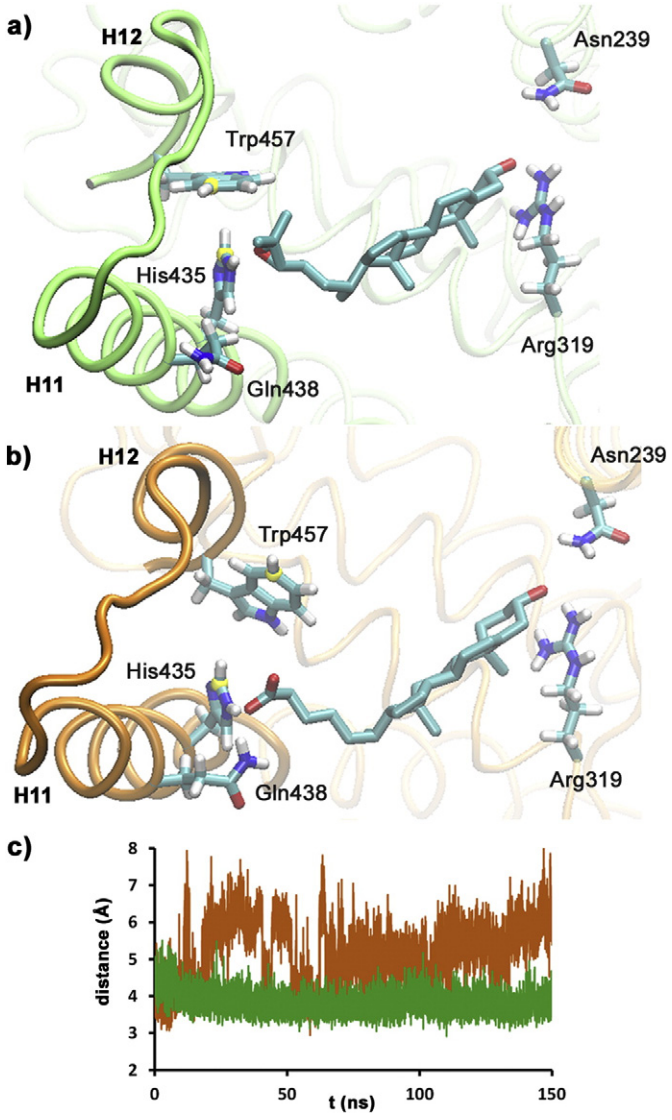

Fig. 1. MD simulations of LXRβ/**1** and LXRβ/**3** complexes. (a–b) Representative snapshot of the ligand binding mode of compound **1** (a) and compound **3** (b); (c) time evolution of distance between CE1 atom of His435 and CZ3 atom of Trp457 in the LXRβ/**1** (green) and in the LXRβ/**3** (orange) complexes.

state of NRs by modulating the overall shape of the NR AF-2 domain involved in the interaction with co-factors. Thus, by constraining the position of His435, a ligand can indirectly promote the orientation of Trp457 to maintain the H12 in an agonistic position. According to the MD trajectory, the time evolution distance between the CE1 atom of His435 and the CZ3 atom of Trp457 reveals a tightly T-shaped

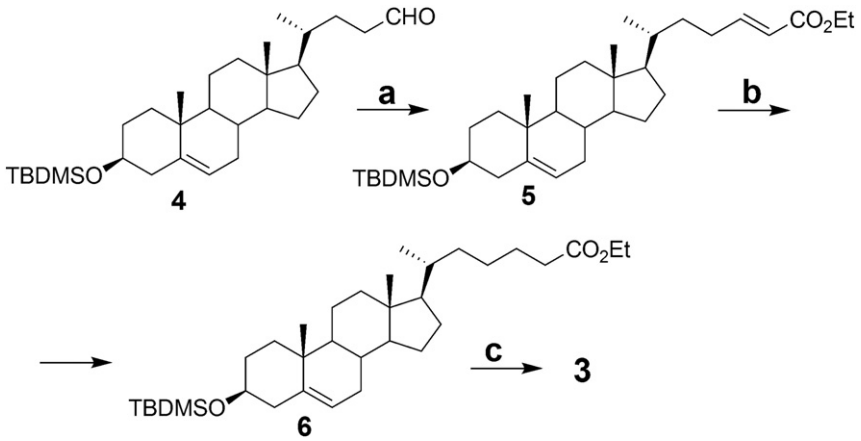

Scheme 1. Synthesis of compound **3**. Reagents and conditions: (a) [$Ph_3PCH_2CO_2Et$]Br, CH_2Cl_2-$NaHCO_3$ (aq), reflux (60%); (b) i) H_2, 10% Pd/C, EtOAc, 1 bar, 25 °C (98%); (c) i) HF 40%, THF-CH_3CN, 0 °C (90%), ii) LiOH, MeOH-THF-H_2O (92%).

aromatic–aromatic interaction between these residues in the LXRβ/**1** system (Fig. 1c). Consistently with the proposed model, the H12 of this complex conserves its original active conformation during the time-scale of the simulation. On the other hand, the geometry of the His435–Trp457 interaction results severely altered in the LXRβ/**3** trajectory (Fig. 1c). In fact, the relative orientation of His435 and Trp457 observed in the agonist **1** system is not maintained in the LXRβ/**3** complex. Consequently, Trp457 acquires more flexibility and other χ_1 rotamers are explored (Fig. S4). Remarkably, the disruption of this H11–H12 interaction observed in the LXRβ/**3** complex produces severe structural changes not only in the overall conformation of H12, but also in the H11–H12 loop which results are considerably affected (Fig. 3). A higher fluctuation of these regions in the presence of compound **3** is evident from the overall backbone fluctuation of the protein (RMSF) over the last 100 ns of the MD simulation depicted in Fig. 4a. The RMSF provides a time-average representation of per-residue fluctuation. A principal component analysis (PCA) of trajectories revealed that significant differences exist when comparing the configurational space sampled by the LXRβ/**1** and LXRβ/**3** systems. Thus, the LXRβ/**3** complex samples a more extended area, indicating that this ligand induces dynamical alterations of the receptor backbone to a larger extent than the agonist **1** (Fig. 4b and c). Based on these results, we propose that the presence of compound **3** is not compatible with an active LXRβ conformation; this is associated with the inverse agonist effect of compound **3** observed in the transactivation activity assays.

Taking into account these findings, the LXRβ/**2** complex was also simulated by introducing the C-25 methyl group into the initial LXRβ/**3** system. The resulting trajectory showed a well-defined ligand binding mode, with the C-27 carboxylic group strongly contacting both His435 and Gln438 residues (Fig. S1c). Contrary to the LXRβ/**3** system, where

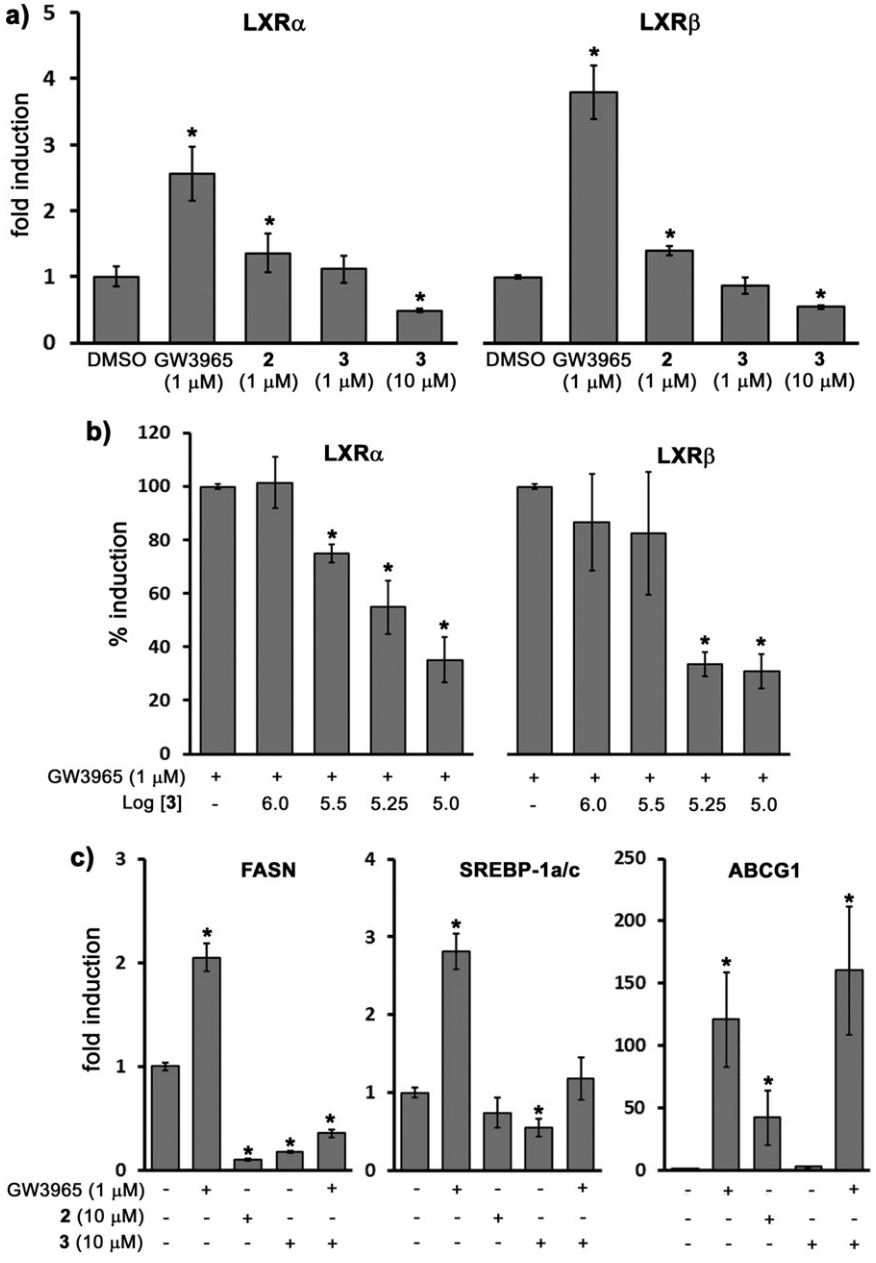

Fig. 2. Biological activity of compound **3**. (a–b) HEK-293 T cells were cotransfected with pLRE-LUC, pRXR and pLXRα or pLXRβ vectors and then incubated for 18 h as indicated. Luciferase activity was measured and normalized with β-galactosidase activity. (a) Values are expressed as fold induction relative to the control (DMSO); (b) values are expressed as % induction relative to GW3965. (c) FASN, SREBP-1a/c, and ABCG1 expression were evaluated in HepG2 cells incubated for 24 h as indicated. Total RNA was extracted and quantified by RT-qPCR. Values are expressed as fold induction relative to the control (DMSO). Means ± S.E. from three independent experiments are shown. *$p < 0.05$ vs control (DMSO).

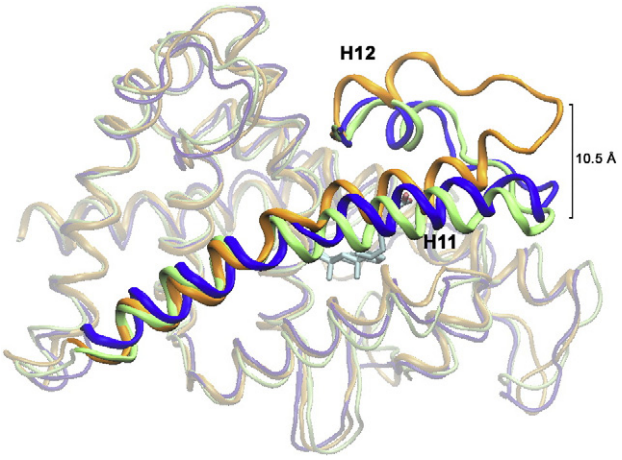

Fig. 3. Superposition of LXRβ/**1** (green), LXRβ/**2** (blue) and LXRβ/**3** (orange) complexes, from representative snapshots of the molecular dynamics simulations. Only compound **3** is shown in the LBP for clarity.

a fully extended conformation of the steroid side chain is favored, the side chain of compound **2** adopted a torsioned conformation, with torsion angles d_1 and d_2 fluctuating roughly around 180° and 60°, respectively (Fig. S1f). This corresponds to a global conformation of the steroid side chain similar to that observed in the LXRβ/**1** system. Regarding the His435 and Trp457 residues, the time evolution of the CE1–CZ3 distance was conserved, indicating that the original orientation was preserved (Fig. S5). Moreover, the Trp457 remained in the same the χ_1 rotamer, similar to the LXRβ/**1** system (Fig. S4d). Consistently, the H11–H12 loop and the H12 global orientation of LXRβ/**2** complex resulted in a stable active conformation (Fig. 3). Finally, RMSF values and PCA of the trajectory were very similar to those obtained for the agonist LXRβ/**1** system (Fig. 4). These results strongly suggest that the C-25 methyl plays a key role in maintaining a torsioned side chain conformation, able to stabilize an active LXRβ state.

2.4. Cofactor recruitment of the LXRβ/3 complex

Both LXR coactivators and corepressors are specifically recognized by the AF-2 domain, which is formed by residues of H3, H4 and H12 [18–20]. Coactivators such as NCoA1 and NCoA2 contain multiple LxxLL (NR boxes), while NR corepressors such as NCoR1 and NCoR2 contain multiple I/LXXII motifs (CoRNR boxes). To further investigate the molecular basis of the inverse agonism of compound **3**, and taking advantage of the fact that the LXRβ LBD/**1** complex has been crystallized together with a peptide derived from box-2 of NCoA1 (residues 682–697), we constructed the corresponding LXRβ/ligand/$NCoA1_{682-697}$ complexes for compounds **1**–**3** and ran 150 ns MD simulations for each case. We observed a stable interaction between the LXRβ and the coactivator peptide in the presence of both compound **1** and compound **2**, with small values of the root mean squared deviation (RMSD) of the peptide backbone atoms throughout the MD trajectories (Fig. 5a). In contrast, when compound **3** is bound, the receptor–peptide interaction appears strongly destabilized, with the peptide exploring several different conformations while large RMSD values are observed (Fig. 5a). The disturbance in the original conformation of the $NCoA1_{682-697}$ peptide may be clearly seen by superimposing snapshots taken at each nanosecond of the MD simulation, on the final LXRβ LBD structures (Fig. 5b–d). As an additional control, we also constructed and simulated the LBD/GW3965/$NCoA1_{682-697}$ complex, finding a very stable binding of the peptide, which is associated with the strong agonism of GW3965 (Fig. S5). In this way, according to the above findings, the presence of compound **3** would not be compatible with a proper recruitment of this coactivator NR-box.

Recently, using a TR-FRET coactivator assay, Theofilopoulos et al. reported that compound **2** increases the binding of a synthetic coactivator peptide by the LXRβ [17], a result consistent with the above MD

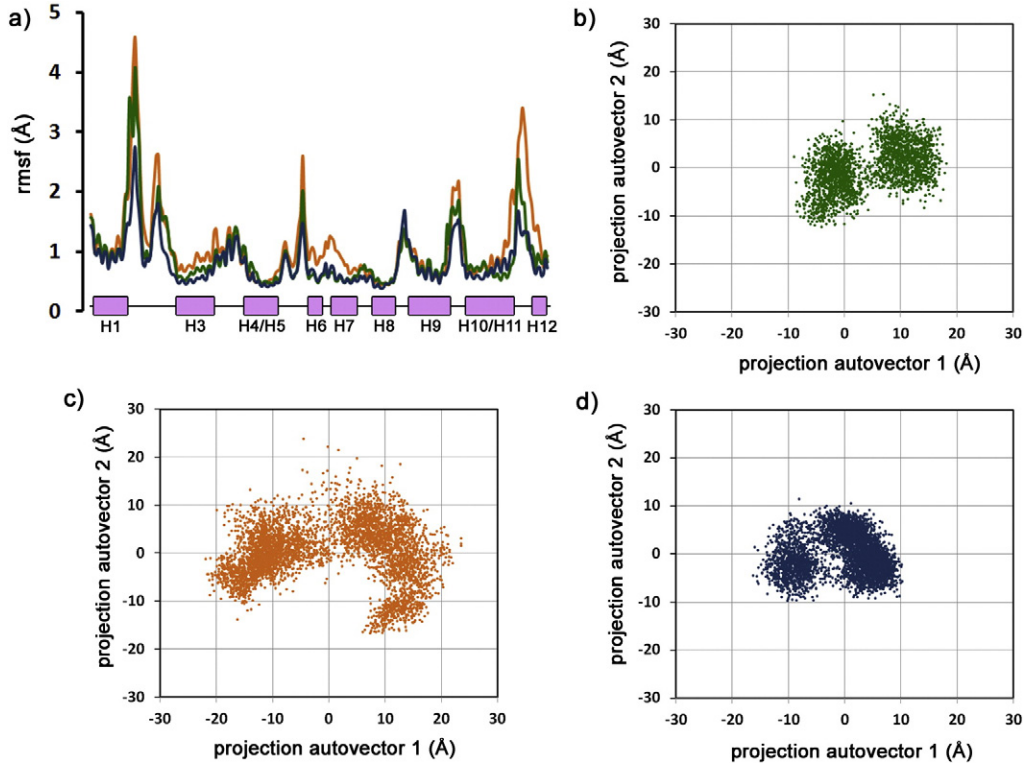

Fig. 4. a) RMSF values of the LXRβ/**1** (green), LXRβ/**3** (orange) and LXRβ/**2** (blue) complexes. The secondary structure of LXRβ LBD is schematized along the *x*-axis. b–d) Principal Component Analysis of MD trajectories: projection on the first two eigenvectors in the LXRβ/**1** (b), LXRβ/**3** (c) and LXRβ/**2** (d) complexes.

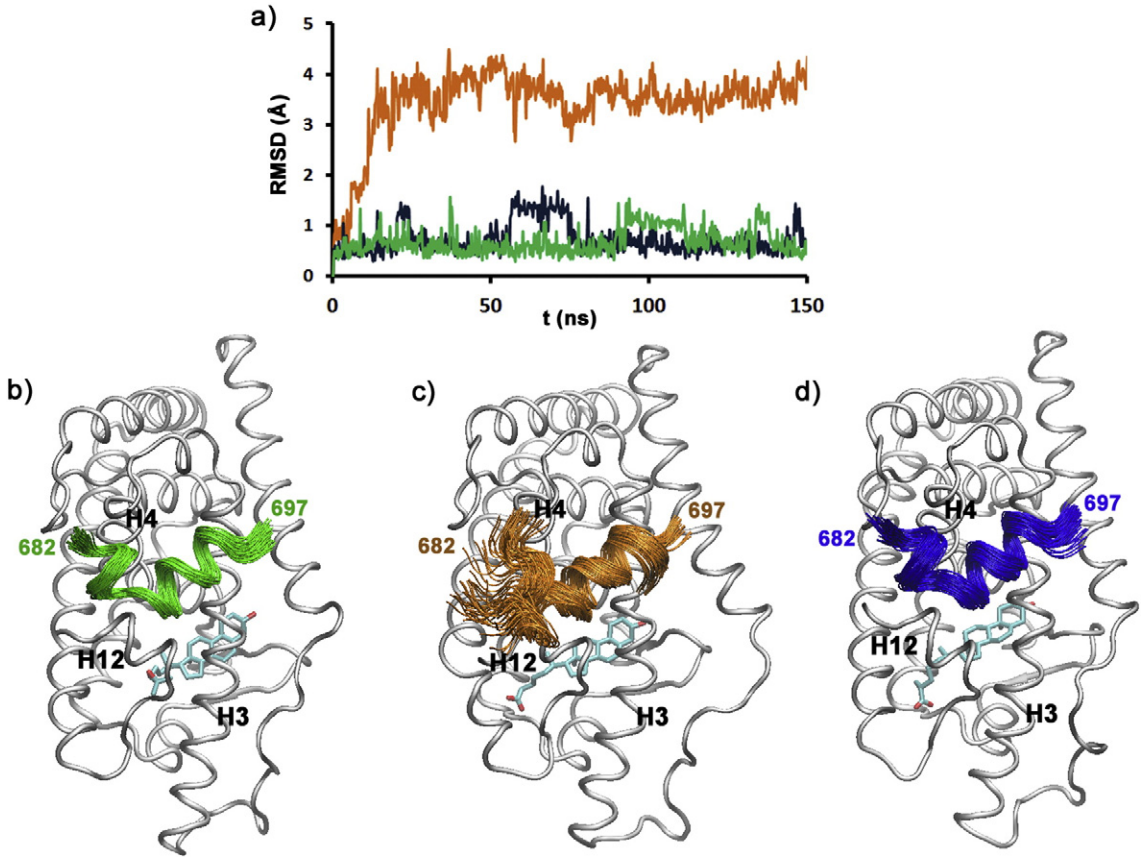

Fig. 5. a) Temporal evolution of the RMSD values of the LXRβ/**1**/NCoA1$_{682-697}$ (green), LXRβ/**3**/NCoA1$_{682-697}$ (orange) and LXRβ/**2**/NCoA1$_{682-697}$ (blue) complexes. b–d) Superposition of snapshots of the NCoA1 peptide on the final LXRβ structure of each system: b) LXRβ/**1**/NCoA1$_{682-697}$, c) LXRβ/**3**/NCoA1$_{682-697}$ and d) LXRβ/**2**/NCoA1$_{682-697}$.

simulation for this compound (Fig. 5d). Then to assess the ability of compound **3** to favor binding of NR cofactors to the LXRβ we used the *in vitro* Marconi assay [21]. Thus, the interaction between GST-LXRβ LBD/GW3965 or the GST-LXRβ LBD/**3** complexes and peptides corresponding to box-2 and box-3 of NCoA1 and NoCA2 or box-1 and box-2 of NCoR1 and NCoR2 was determined. Results showed that the presence of the strong agonist GW3965 led to an increase in the binding of LXR to all coactivator peptides, compared to the unliganded receptor. On the other hand, compound **3** considerably decreased recruitment of coactivators (Fig. 6a). In particular, results corresponding to box-2 of the NCoA1 are in agreement with the MD results obtained for these complexes.

When we evaluated the binding of LXRβ complexes to CoRNR motifs, we found a significant difference between the interactions of either NCoR1 box-2 or NCoR2 box-1 peptides with LXRβ/GW3965 and LXRβ/**3** complexes. In fact, GW3965 produced a small decrease of peptide binding while compound **3** markedly increased the recruitment of these peptides by LXRβ (Fig. 6b). On the other hand, no differences between both complexes were observed in the binding of NCoR1 box-1 and NCoR2 box-2 peptides. These results support the hypothesis that compound **3** induces conformational changes on the LXRβ AF-2 domain that would favor corepressor over coactivator recruitment.

3. Conclusion

Although the final LXR outcome depends on multiple actors, the structure and the concentration of specific ligands are critical determinants. In the particular case of steroids with a hydroxylated side chain, modifications at the position of the polar group strongly affect the LXR functionality, suggesting that different hot spots would be involved in the receptor/steroid recognition. Even small structural changes, such as the inversion of the C-22 configuration may flip a full agonism into antagonism. Similarly, we have demonstrated that the simple removal of the C-25 methyl moiety of cholestenoic acid also provokes a drastic change in the LXR activity profile. Alteration of the receptor behavior due to modifications of the polar groups is usually explained by considering that these groups specifically interact with polar receptor residues that in turn, control the activation state of the complex. However, since methyl groups are involved in non-specific interactions, other molecular determinants must be considered to explain their influence on the receptor activity.

On the basis of theoretical studies, we propose that conformation differences on the steroid side chain might explain this effect. When the C-25 methyl moiety is present, the steroid side chain acquires a torsioned conformation that allows for a proper interaction between residues His435 and Trp457. The latter interaction is responsible for the stabilization of helix-12 in an agonist orientation. Conversely, in the 27-nor analog a fully extended side chain is favored, impairing the aromatic–aromatic His435/Trp457 interaction and thus destabilizing the active conformation of the receptor. According to the experimental results, the antagonist action of **3** could reside in the ability of the LXRβ/ligand complex to better interact with corepressors than coactivators, supporting the idea that this compound favors a complex inactive state.

In a recent work, Flaveny et al. have shown that inactivation of the LXR by a non-steroidal LXR inverse agonist alters the expression levels of glycolitic and lipogenic enzymes, provoking cell death in tumor cells without affecting cell viability in non-malignant cells [22]. Notably, an important anti-tumor activity without toxicity, inflammation or weight loss was observed for that compound, suggesting that LXR inverse agonists may represent a new type of anti-cancer drugs [22]. Several non-steroidal LXR inverse agonists have been reported but steroidal ones are still rare. From a synthetic standpoint, steroids with

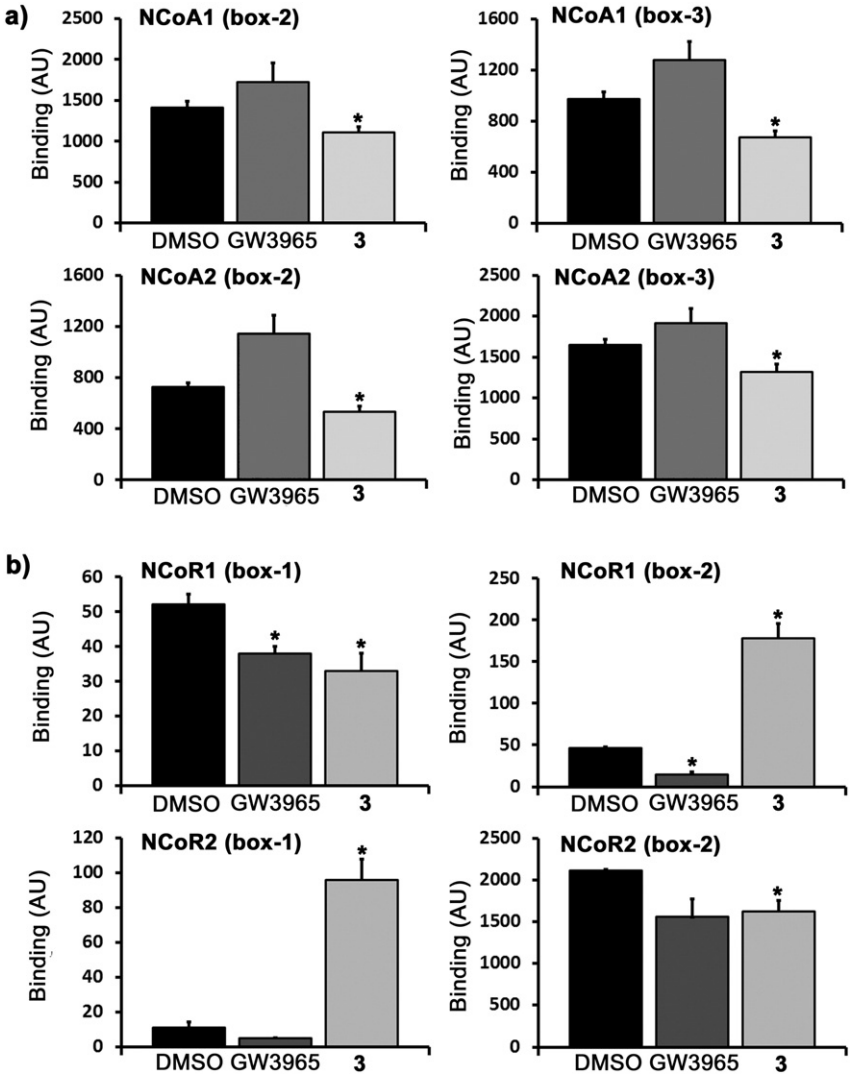

Fig. 6. Functional comparison of LXR ligands using MARCoNI. GST-tagged LXRβ-LBD was incubated on a peptide microarray with 154 unique coregulator-derived sequences, on the presence or absence (DMSO) of 10 μM GW3965 or compound **3**. LXRβ-peptide binding is represented as Arbitrary Units fluorescence of ALEXA488-conjugated GST antibody quantified by CCD camera. Means ± S.E. from three independent experiments with the indicated coactivator NR-boxes (a) or corepressor CoRNR-boxes (b) are shown.* $p < 0.05$ vs Control (DMSO).

a linear (unbranched) side chain are more accessible than those with a C-25 stereocenter, thus the fact that a 27-nor steroid can be recognized by the receptor increases the number of potential structures with the ability to act as LXR ligands, providing a new entry for the design of LXR inhibitors with potential applications in cancer treatments.

4. Materials and methods

4.1. Chemical synthesis

4.1.1. General

NMR spectra were recorded on a Bruker Avance II 500 NMR spectrometer (^{1}H at 500.13 MHz, ^{13}C at 125.77 MHz) in deuterochloroform. Chemical shifts are given in ppm downfield from TMS as internal standard, and *J* values are given in Hz. Multiplicity determinations and 2D spectra (COSY, NOESY, HSQC and HMBC) were obtained using standard Bruker software. Exact mass spectra were obtained using a Bruker micrOTOF-Q II mass spectrometer, equipped with an ESI source operating in positive mode. Flash column chromatography was carried out on silica gel S 0.040–0.063 mm. Thin layer chromatography (tlc) analysis was performed on silica gel 60F254 (0.2 mm thick). The homogeneity of all compounds was confirmed by tlc. Solvents were evaporated at reduced pressure and ca. 40–50 °C. Cholenaldehyde **4** was obtained following the procedure described previously by us [16].

4.1.2. 3β-(t-Butyldimethylsilyloxy)-27-nor-5,24-cholestadien-26-oic acid ethyl ester (**5**)

A saturated aqueous solution of $NaHCO_3$ (1 mL) was heated to 100 °C and poured over a mixture of cholenaldehyde **4** (50 mg, 0.106 mmol) dissolved in dichloromethane (2 mL), and $[Ph_3PCH_2CO_2Et]Br$ (55 mg, 0.127 mmol). The reaction mixture was stirred at 50 °C for 2 h, allowed to cool to room temperature and extracted with dichloromethane. The organic layer was dried with sodium sulfate and the solvent evaporated under vacuum. The resulting solid was purified by flash chromatography (hexane-ethyl acetate 97:3 → 90:10) to give **5** as a *E*/*Z* mixture (5:1) (34.7 mg, 60%).

E isomer: ^{1}H NMR δ 6.96 (1H, dt, J = 15.6 and 7.0 Hz, H-24), 5.81 (1H, dt, J = 15.6 and 7.0 Hz, H-25), 5.31 (1H, dt, J = 5.1 and 1.8 Hz, H-6), 4.18 (2H, q, J = 7.1 Hz, O**C**$\mathbf{H}_2$CH$_3$), 3.48 (1H, tt, J = 11.0 and 4.8 Hz, H-3), 2.27 (1H, m, H-4β), 2.26 (1H, m, H-23a), 2.18 (1H, ddd, J = 2.1, 4.8, 13.3 Hz, H-4α), 2.09 (1H, m, H-23b), 2.00 (1H, dt, J = 12.2 and 3.4 Hz, H-12β), 1.97 (1H, m, H-7β), 1.83 (1H, m, H-16α), 1.81 (1H, m, H-1β), 1.71 (1H, m, H-2β), 1.59 (1H, m, H-15β), 1.55 (1H, m, H-22a), 1.54 (2H, m, H-2α and H-7α), 1.48 (2H, m, H-11), 1.45 (1H, m, H-8), 1.44 (1H, m, H-20), 1.29 (3H, t, J = 7.2 Hz,

$OCH_2C\mathbf{H}_3$), 1.27 (1H, m, H-16β), 1.18 (1H, m, H-22b), 1.17 (1H, dt, J = 4.7 and 12.8 Hz, H-12α), 1.11 (1H, m, H-17), 1.08 (1H, m, H-15α), 1.05 (1H, m, H-1α), 1.00 (3H, s, H-19), 0.99 (1H, m, H-14), 0.94 (3H, d, J = 6.5 Hz, H-21), 0.92 (1H, m, H-9), 0.89 (9H, s, $(CH_3)_3C$-Si)), 0.67 (3H, s, H-18), 0.06 (6H, s, $(CH_3)_2$-Si.

^{13}C NMR δ 166.8 (C-26), 150.0 (C-24), 141.6 (C-5), 121.1 (C-6), 121.0 (C-25), 72.6 (C-3), 60.1. ($O\mathbf{C}H_2CH_3$), 56.8 (C-14), 55.9 (C-17), 50.2 (C-9), 42.8 (C-4), 42.4 (C-13), 39.8 (C-12), 37.4 (C-1), 36.6 (C-10), 35.5 (C-20), 34.3 (C-22), 32.1 (C-2), 31.90 (C-7), 31.89 (C-8), 30.0 (C-23), 28.2 (C-16), 25.9 (($\mathbf{C}H_3)_3C$-Si), 24.2 (C-15), 21.0 (C-11), 19.4 (C-19), 18.5 (C-21), 18.3 (($CH_3)_3\mathbf{C}$-Si), 14.3 ($OCH_2\mathbf{C}H_3$), 11.9 (C-18), −4.6 (($CH_3)_2$-Si); ESI HRMS: m/z calcd for $C_{34}H_{58}NaO_3Si$ $[M + Na]^+$ 565.4047, found 565.4049.

*4.1.3. 3β-(t-Butyldimethylsilyloxy)-27-nor-5-cholesten-26-oic acid ethyl ester (**6**)*

To a solution of **5** (34 mg, 0.063 mmol) in ethyl acetate (6.5 mL) Pd/C 10% *w*/*w* (6.9 mg) was added and the resulting mixture was hydrogenated at 1 atm and room temperature for 1 h. The reaction mixture was then filtered through a silica gel pad, washing the filter with ethyl acetate. The filtrate was evaporated under reduced pressure to give **6** (33.4 mg, 98%).

^{1}H NMR): δ 5.31 (1H, dt, J = 5.3 and 1.8 Hz, H-6), 4.12 (2H, d, J = 7.0 Hz, $OC\mathbf{H}_2CH_3$), 3.48 (1H, tt, J = 11.0 and 4.7 Hz, H-3), 2.28 (2H, m, H-25), 2.26 (1H, H-4β), 2.21 (1H, m, H-23a), 2.16 (1H, ddd, J = 13.3, 4.8 and 2.2 Hz, H-4α), 1.99 (1H, dt, J = 12.2 and 3.4 Hz, H-12β), 1.97 (1H, m, H-7β), 1.82 (1H, m, H-16α), 1.80 (1H, dt, J = 13.2 and 3.5 Hz, H-1β), 1.71 (1H, m, H-2α), 1.61 (1H, m, H-24a), 1.58 (1H, m, H-15β), 1.55 (1H, m, H-24b), 1.53 (1H, m, H-2β), 1.52 (1H, m, H-7α), 1.48 (2H, m, H-11), 1.45 (1H, m, H-8), 1.40 (1H, m, H-20), 1.37 (1H, m, H-23b), 1.26 (3H, t, J = 7.0 Hz, $OCH_2C\mathbf{H}_3$), 1.25 (1H, m, H-16β), 1.14 (1H, dt, J = 4.6 and 12.7 Hz, H-12α), 1.04 (3H, m, H-1α and H-22), 1.08 (1H, m, H-17), 1.07 (1H, m, H-15α), 0.91 (1H, m, H-9), 1.00 (3H, s, H-19), 0.91 (3H, d, J = 6.6 Hz, H-21), 0.89 (9H, s, $(CH_3)_3C$-Si)), 0.67 (3H, s, H-18), 0.06 (6H, s, $(CH_3)_2$-Si).

^{13}C NMR δ 173 9 (C-26), 141.6 (C-5), 121.1 (C-6), 72.6 (C-3), 60.1 ($O\mathbf{C}H_2CH_3$), 56.8 (C-14), 56.0 (C-17), 50.2 (C-9), 42.8 (C-4), 42.3 (C-13), 39.8 (C-12), 37.4 (C-1), 36.60 (C-10), 35.6 (C-20), 35.5 (C-22), 34.5 (C-25), 32.1 (C-2), 31.93 (C-7), 31.90 (C-8), 28.2 (C-16), 25.9 (($\mathbf{C}H_3)_3C$-Si), 25.6 (C-23), 25.4 (C-24), 24.3 (C-15), 21.1 (C-11), 19.4 (C-19), 18.6 (C-21), 18.2 ($(CH_3)_3\mathbf{C}$-Si), 14.3 ($OCH_2\mathbf{C}H_3$), 11.8 (C-18), −4.6 (($CH_3)_2$-Si); ESI HRMS: m/z calcd for $C_{34}H_{60}NaO_3Si$ $[M + Na]^+$ 567.4204, found 567.4190.

*4.1.4. 3β-Hydroxy-27-nor-5-cholesten-26-oic acid (**3**)*

To a solution of **6** (33 mg, 0.061 mmol) in THF (2.7 mL) and acetonitrile (2.7 mL), was added 40% hydrofluoric acid (2.2 mL) and the solution was stirred for 1 h at 0 °C. The reaction mixture was neutralized with aqueous potassium bicarbonate and then extracted with ethyl acetate. The organic layer was washed with water, dried with sodium sulfate and the solvent evaporated under vacuum to give the 3β-hydroxysteroid; ^{1}H NMR δ 5.36 (1H, dt, J = 5.2 and 2.1 Hz, H-6), 4.13 (2H, t, J = 7.0 Hz, $OC\mathbf{H}_2CH_3$), 3.53 (1H, tt, J = 11.3 and 4.3 Hz, H-3), 2.29 (3H, m, H-25 and H-4β), 2.24 (1H, m, H-4α), 2.01 (1H, dt, J = 12.6 and 3.4 Hz, H-12β), 1.99 (1H, m, H-7β), 1.85 (1H, m, H-1β), 1.84 (1H, m, H-2α), 1.83 (1H, m, H-16α), 1.59 (2H, m, H-24), 1.58 (1H, m, H-15β), 1.55 (1H, m, H-7α), 1.51 (1H, m, H-2β), 1.50 (1H, m, H-11β), 1.46 (1H, m, H-11α), 1.45 (1H, m, H-8), 1.40 (1H, m, H-20), 1.38 (1H, m, H-23a), 1.26 (1H, m, H-16β), 1.26 (3H, t, J = 7.0 Hz, $OCH_2C\mathbf{H}_3$), 1.22 (1H, m, H-23b), 1.15 (1H, m, H-12α), 1.09 (1H, m, H-17), 1.08 (1H, m, H-15α and H-1α), 1.04 (2H, m, H-22), 0.99 (1H, m, H-14), 0.93 (1H, m, H-9), 1.01 (3H, s, H-19), 0.91 (3H, d, J = 6.6 Hz, H-21), 0.68 (3H, s, H-18).

^{13}C NMR δ 174.0 (C-26), 140.8 (C-5), 121.7 (C-6), 71.8 (C-3), 60.2 ($O\mathbf{C}H_2\mathbf{C}H_3$), 56.8 (C-14), 56.0 (C-17), 50.1 (C-9), 42.32 (C-13), 42.29 (C-4), 39.8 (C-12), 37.2 (C-1), 36.5 (C-10), 35.6 (C-20), 35.5 (C-22), 34.5 (C-25), 31.9 (C-7), 31.7 (C-8), 31.7 (C-2), 28.2 (C-16), 25.6 (C-23), 25.4 (C-24), 24.3 (C-15), 21.1 (C-11), 19.4 (C-19), 18.6 (C-21), 14.3 ($OCH_2\mathbf{C}H_3$), 11.9 (C-18).

To a solution of the ethyl ester obtained above (23.5 mg, 0.055 mmol) in a mixture of tetrahydrofuran/methanol (1:1) (1.8 mL), 5% aqueous lithium hydroxide (0.30 mL) was added. After stirring at room temperature for 3 h, water was added (3 mL), the mixture was acidified with 1 N HCl (to pH 3), concentrated to a third of its volume and then extracted with ethyl acetate. The combined organic layers were dried with magnesium sulfate and the solvent was evaporated. The resulting solid was purified by flash chromatography (hexane-ethyl acetate 60:40) to give **3** (20.4 mg, 83% from **6**); ^{1}H NMR δ 5.35 (1H, dt, J = 5.1 and 2.0 Hz, H-6), 3.53 (1H, tt, J = 11.2 and 4.8 Hz, H-3), 2.35 (2H, m, H-25), 2.30 (1H, ddd, J = 13.2, 5.2, 1.8 Hz, H-4α), 2.23 (1H, br ddd, J = 13.3, 11.1, 2.1 Hz, H-4β), 2.00 (1H, dt, J = 12.6 and 3.3 Hz, H-12β), 1.97 (1H, ddt, J = 17.1, 2.6, 5.1 Hz, H-7β), 1.84 (1H, m, H-1β), 1.83 (1H, m, H-16α), 1.81 (1H, m, H-2α), 1.63 (1H, m, H-24a), 1.57 (1H, m, H-15β), 1.57 (1H, m, H-24b), 1.52 (1H, m, H-7α), 1.48 (3H, m, H-2β and H-11), 1.44 (1H, m, H-8), 1.39 (1H, m, H-20), 1.39 (1H, m, H-23a), 1.24 (1H, m, H-16β), 1.23 (1H, m, H-23b), 1.15 (1H, dt, J = 4.7 and 12.8 Hz, H-12α), 1.08 (1H, m, H-17), 1.07 (2H, m, H-15α and H-1α), 1.03 (2H, m, H-22), 1.01 (3H, s, H-19), 0.98 (1H, m, H-14), 0.92 (1H, m, H-9), 0.91 (3H, d, J = 6.6 Hz, H-21), 0.68 (3H, s, H-18).

^{13}C NMR δ 176.8 (C-26), 140.8 (C-5), 121.7 (C-6), 71.8 (C-3), 56.8 (C-14), 56.0 (C-17), 50.1 (C-9), 42.34 (C-13), 42.30 (C-4), 39.8 (C-12), 37.3 (C-1), 36.5 (C-10), 35.6 (C-20), 35.5 (C-22), 33.6 (C-25), 31.9 (C-8 and C-7), 31.7 (C-2), 28.2 (C-16), 25.6 (C-23), 25.2 (C-24), 24.3 (C-15), 21.1 (C-11), 19.4 (C-19), 18.7 (C-21), 11.9 (C-18); ESI HRMS: m/z calcd for $C_{26}H_{42}NaO_3$ $[M + Na]^+$ 425.3026, found 425.3023.

4.2. Biological methods

4.2.1. Transactivation activity

HEK-293 T cells were cultured at 37 °C under 5% CO_2 humidified atmosphere in DMEM supplemented with 10% fetal calf serum (FCS) containing penicillin (100 IU/mL), streptomycin (100 mg/mL) and glutamine (2 mM) in p100 plates. For transient transfections, 3×10^5 cells were plated in 12-well plates and transfected with Lipofectamine according to the manufacturer's protocol (Lipofectamine 2000, Invitrogen). Analyses of human LXRα and LXRβ activities were performed by transfecting 0.7 μg of the reporter construct pLRE-LUC, 0.6 μg of the respective pLXRα or pLXRβ expression vector (kindly provided by Dr. Shutsung Liao, University of Chicago), 0.2 μg of human pRXR and 0.6 μg of pRSV-LacZ (Clontech Inc., Palo Alto, CA) as control of transfection. After transfection, the medium was replaced by serum-free medium containing antibiotics. Cells were then incubated for 18 h with GW3965 (Sigma), compound **2** (Avanti Polar Lipids, Inc.) or compound **3** at the concentrations indicated. Ligands were used from 1000-fold stock solutions in dimethylsulfoxide (DMSO). Incubations were stopped by aspirating the medium and washing the cells twice with phosphate buffered saline solution (PBS). Cells were then harvested in lysis buffer and luciferase activity was measured according to the manufacturer's protocol (Promega Inc.). β-Galactosidase activity was measured as previously described [23].

4.2.2. FASN, SREBP-1a/c and ABCG1 expression levels by mRNA analysis

HepG2 cells were cultured at 37 °C under 5% CO_2 humidified atmosphere in high glucose DMEM supplemented with 10% fetal calf serum (FCS) containing penicillin (100 IU/mL), streptomycin (100 mg/mL) and glutamine (2 mM) in p100 plates. 5×10^5 cells were plated in p6 plates and incubated for 48 h. Then cells were incubated with steroids at the indicated concentrations in serum-free medium containing antibiotics for 24 h. Steroids were used from 1000-fold stock solutions in DMSO. Total RNA was extracted with TRIzol reagent according to the manufacturer's instructions (Invitrogen). For reverse transcription, 1 μg of RNA was used. The first cDNA strand was synthesized with

200 U MMLV reverse transcriptase (Promega, Inc.), 25 ng/L random primers (Invitrogen), 2 g/L Rnasin (Promega, Inc.) and 1.5 mM dNTPs (Invitrogen). Reverse transcription was performed at 72 °C for 5 min followed by 1 h at 37 °C and finally 5 min at 95 °C. For quantitative real-time polymerase chain reaction (qPCR), 25 ng of cDNA was used. All reactions were conducted in a volume of 25 μL containing 4 mM $MgCl_2$, 0.2 mM dNTPs (Invitrogen), 0.75 U Taq polymerase (Invitrogen), 1/30,000 Sybr Green (Roche) and specific oligonucleotides for *FASN*, *SREBP-1a/c* and *ABCG1* genes in a DNA Engine Opticon instrument (MJ Research). Reactions were run for 40 cycles under the following conditions: 15 s at 94 °C, 20 s at 66 °C and 25 s at 72 °C. The amplification of unique products in each reaction was verified by melting curve and ethidium bromide (Sigma Aldrich) stained 2% agarose gel electrophoresis. *FASN*, *SREBP-1a/c* and *ABCG1* expression levels were normalized to GAPDH expression by qRT-PCR performed with specific oligonucleotides by using a standard curve method. Primer sequences are available upon request.

4.2.3. Cell viability assay

5000 HepG2 cells were cultured in 96-well flat bottomed microtiter plates at 37 °C under 5% CO_2 humidified atmosphere for 48 h. Then cells were incubated with steroids at the indicated concentrations in medium free of phenol red containing antibiotics for further 24 h. Steroids were used from 1000-fold stock solutions in DMSO. Medium was removed and replaced by 100 μL of fresh medium and 10 μL of MTT solution 12 mM (3-(4,5-dimethylthiazol-2-yl)-2,5-diphenyltetrazolium bromide) for 2 h. After that, MTT solution was removed and DMSO (50 μL) was added and incubated at 37 °C for 10 min to dissolve the formazan crystals. Absorbance was read by microplate reader with 540/655 nm double wavelength.

4.2.4. Microarray assay for real-time coregulator–nuclear receptor interaction (MARCoNI)

LXRβ–coregulator interaction and modulation thereof by compounds was assessed using MARCoNI on PamChip microarrays as described previously [21] using a PamStation®-12 (PamGene). In short, assay mixtures were prepared on ice with a 5 nM concentration of glutathione-S-transferase (GST)-tagged human LXRβ-LBD (PV4659, (Invitrogen), 25 nM of Alexa488-conjugated GST antibody (Invitrogen) and TR-FRET Coregulator Buffer I (PV4662, Invitrogen) in the presence of 10 μM compound or solvent (DMSO, 2% final concentration) only. Initial blocking was performed by incubating the peptide microarray for 20 cycles (two cycles per minute) with 25 μL blocking buffer (TBS with 1% BSA and 0.01%, Tween-20). Subsequently, blocking buffer was removed and 25 μL assay mix was transferred to the array and incubated for 80 cycles at 20 °C. After removal of the unbound receptor by aspiration and subsequent rinsing of the arrays with 25 μL TBS, a tiff image of each array was obtained by a CCD camera.

Image analysis was performed using BioNavigator software (PamGene), which applies automated array grid finding and subsequent quantification of signal and local background for each individual peptide. In short, the boundaries of a spot are determined and the median fluorescent signal was quantified within the spot (signal) as well as that in a defined area surrounding it (background). The signal-minus-background value was subsequently used as the quantitative parameter of binding. Individual receptor–peptide binding was calculated as mean ± S.E. from three separate arrays for each condition. Results from peptides corresponding to box-2 (residue 677 to 700) and box-3 (residue 737 to 759) of NCoA1 (UniProt Accession: Q15788), box-2 (residue 677 to 700) and box-3 (residue 733 to 755) of NCoA2 (UniProt Accession: Q15596), box-1 (residue 1925 to 1946) and box-2 (residue 2039 to 2061) of NCoR1 (UniProt Accession: O75376) and box-1 (residue 2123 to 2145) and box-2 (residue 2330 to 2352) of NCoR2 (UniProt Accession: Q9Y618) are shown. Significance (p) of compound-mediated alteration of binding was assessed using unpaired Student's t-test assuming equal variance.

4.3. Computational methods

4.3.1. Initial structures of LXRβ/ligand complexes

The starting coordinates of the LXRβ ligand binding domain were taken from the crystal structure of the LXRβ/**1** complex (pdb: 1p8d, chain A). The missing residues of H1–H3 loop (255–258) were added with the Modeler program [24]. In order to build the LXRβ/**3** complex, the HF/6-31G** optimized structure of compound **3** was introduced by superimposing the skeleton carbon atoms with the corresponding atoms of **1**. The LXRβ/**2** complex was obtained from LXRβ/**3** coordinates adding the C-25 methyl group in the *R* configuration and deleting the corresponding hydrogen atom. The corresponding force field parameters of the ligand, RESP (restraint electrostatic potential) atomic partial charges were computed using the HF/6-31G** method in the quantum chemistry program Gaussian 03 [25] for the corresponding optimized structures. The LXRβ/$NCoA1_{682–697}$ complexes were constructed.

4.3.2. Initial structures of LXRβ/ligand/$NCoA1_{682–697}$ complexes

These complexes were constructed from the abovementioned initial structures adding the coordinates of the $NCoA1_{682–697}$ peptide (pdb: 1p8d, chain C). The LXRβ/GW3965 was constructed by superimposing the protein backbone with the protein backbone of pdb: 4nqa, and extracting the GW3965 coordinates.

4.3.3. Molecular dynamics

Molecular Dynamics (MD) were performed with the AMBER 12 software package [26]. Ligand parameters were assigned according to the general AMBER force field (GAFF) and the corresponding RESP charges using the Antechamber. The Amber99 force field parameters were used for all receptor residues [27]. Complexes were immersed in an octahedral box of TIP3P water molecules using the Tleap module, giving final systems of around 30,000 atoms. Systems were initially optimized and then gradually heated to a final temperature of 300 K. Starting from these equilibrated structures, MD production runs of 150 ns were performed. All simulations were performed at 1 atm and 300 K, maintained with the Berendsen barostat and thermostat respectively, using periodic boundary conditions and the particle mesh Ewald method (grid spacing of 1 Å) for treating long-range electrostatic interactions with a uniform neutralizing plasma. The SHAKE algorithm was used to keep bonds involving H atoms at their equilibrium length, allowing the use of a 2 fs time step for the integration of Newton's equations.

4.4. Statistical analysis

Results are expressed as means ± standard error of at least 3 independent experiments. Statistical analysis was performed with STATISTICA 6.0 (StatSoft Inc.) and consisted in one-way ANOVA followed by Dunnett's multiple comparisons test. Before statistical analysis, Q–Q plot and Shapiro–Wilk's test were performed for normality. Homoscedasticity was assessed with Levene's test. Asterisk means significant differences ($p < 0.05$) versus control.

Transparency document

The Transparency document associated with this article can be found in online version.

Acknowledgments

We thank Dr. Shutsung Liao (University of Chicago) for the pLRE-LUC, pLXRα and pLXRβ vectors. This work was supported by grants from Agencia Nacional de Promoción Científica y Tecnológica (PICT 2010-0623), CONICET-Argentina (PIP 11220110100702) and Universidad de Buenos Aires (Grant N° 20020130100367BA).

Appendix A. Supplementary data

Supplementary data to this article can be found online at http://dx.doi.org/10.1016/j.bbalip.2015.09.007.

References

[1] T. Jakobsson, E. Treuter, J.A. Gustafsson, K.R. Steffensen, Liver X receptor biology and pharmacology: new pathways, challenges and opportunities, Trends Pharmacol. Sci. 33 (2012) 394–404.

[2] C.M. Tice, P.B. Noto, K.Y. Fan, L. Zhuang, D.S. Lala, S.B. Singh, The medicinal chemistry of liver X receptor (LXR) modulators, J. Med. Chem. 57 (2014) 7182–7205.

[3] S.S. Im, T.F. Osborne, Liver X receptors in atherosclerosis and inflammation, Circ. Res. 108 (2011) 996–1001.

[4] E. Viennois, K. Mouzat, J. Dufour, L. Morel, J.M. Lobaccaro, S. Baron, Selective liver X receptor modulators (SLiMs): what use in human health? Mol. Cell. Endocrinol. 351 (2012) 129–141.

[5] C. Hong, P. Tontonoz, Liver X receptors in lipid metabolism: opportunities for drug discovery, Nat. Rev. Drug Discov. 13 (2014) 433–444.

[6] C. Gabbi, M. Warner, J.A. Gustafsson, Action mechanisms of liver X receptors, Biochem. Biophys. Res. Commun. 446 (2014) 647–650.

[7] D. Torocsik, A. Szanto, L. Nagy, Oxysterol signaling links cholesterol metabolism and inflammation via the liver X receptor in macrophages, Mol. Asp. Med. 30 (2009) 134–152.

[8] S. Meaney, A. Babiker, D. Lutjohann, U. Diczfalusy, M. Axelson, I. Bjorkhem, On the origin of the cholestenoic acids in human circulation, Steroids 68 (2003) 595–601.

[9] M. Ogundare, S. Theofilopoulos, A. Lockhart, L.J. Hall, E. Arenas, J. Sjövall, A.G. Brenton, Y. Wang, W.J. Griffiths, Cerebrospinal fluid steroidomics: are bioactive bile acids present in brain? J. Biol. Chem. 285 (2010) 4666–4679.

[10] C. Song, S. Liao, Cholestenoic acid is a naturally occurring ligand for liver X receptor alpha, Endocrinology 141 (2000) 4180–4184.

[11] P. Mahanti, N. Bose, A. Bethke, J.C. Judkins, J. Wollam, K.J. Dumas, A.A.M. Zimmerman, S.L. Campbell, P.J. Hu, A.A. Antebi, F.C. Schroeder, Comparative metabolomics reveals endogenous ligands of DAF-12, a nuclear hormone receptor, regulating *C. elegans* development and lifespan, Cell Metab. 19 (2014) 73–83.

[12] S.P. Mooijaart, B.W. Brandt, E.A. Baldal, J. Pijpe, M. Kuningas, M. Beekman, B.J. Zwaan, P.E. Slagboom, R.G. Westendorp, D. Van heemst, *C. elegans* DAF-12, nuclear hormone receptors and human longevity and disease at old age, Ageing Res. Rev. 4 (2005) 351–371.

[13] L.D. Alvarez, P.A. Manez, D.A. Estrin, G. Burton, The *Caenorhabditis elegans* DAF-12 nuclear receptor: structure, dynamics, and interaction with ligands, Proteins: Struct. Func. Bioinf. 80 (2012) 1798–1809.

[14] G.A. Samaja, O. Castro, L.D. Alvarez, M.V. Dansey, D.S. Escudero, A.S. Veleiro, A. Pecci, G. Burton, 27-nor-Δ^4-dafachronic acid is a synthetic ligand of *Caenorhabditis elegans* DAF-12 receptor, Bioorg. Med. Chem. Lett. 23 (2013) 2893–2896.

[15] S. Williams, R.K. Bledsoe, J.L. Collins, S. Boggs, M.H. Lambert, A.B. Miller, J. Moore, D.D. McKee, L. Moore, J. Nichols, D. Parks, M. Watson, B. Wisely, T.M. Willson, X-ray crystal structure of the liver X receptor beta ligand binding domain: regulation by a histidine-tryptophan switch, J. Biol. Chem. 278 (2003) 27138–27143.

[16] M.V. Dansey, L.D. Alvarez, G. Samaja, D.S. Escudero, A.S. Veleiro, A. Pecci, O.A. Castro, G. Burton, Synthetic DAF-12 modulators with potential use in controlling nematodes life cycle, Biochem. J. 465 (2015) 175–184.

[17] S. Theofilopoulos, W.J. Griffiths, P.J. Crick, S. Yang, A. Meljon, M. Ogundare, S.S. Kitambi, A. Lockhart, K. Tuschl, P.T. Clayton, A.A. Morris, A. Martinez, M. Ashwin Reddy, A. Martinuzzi, M.T. Bassi, A. Honda, T. Mizuochi, A. Kimura, H. Nittono, G. De Michele, R. Carbone, C. Criscuolo, J.L. Yau, J.R. Seckl, R. Schüle, L. Schöls, A.W. Sailer, J. Kuhle, M.J. Fraidakis, J.A. Gustafsson, K.R. Steffensen, I. Björkhem, P. Ernfors, J. Sjövall, E. Arenas, Y. Wang, Cholestenoic acids regulate motor neuron survival via liver X receptors, J. Clin. Invest. 124 (2014) 4829–4842.

[18] X. Hu, S. Li, J. Wu, C. Xia, D.S. Lala, Liver X receptors interact with corepressors to regulate gene expression, Mol. Endocrinol. 17 (2003) 1019–1026.

[19] M. Albers, B. Blume, T. Schlueter, M.B. Wright, I. Kober, C. Kremoser, U. Deuschle, M. Koegl, A novel principle for partial agonism of liver X receptor ligands. Competitive recruitment of activators and repressors, J. Biol. Chem 281 (2006) 4920–4930.

[20] Y.L. Son, Y.C. Lee, Molecular determinants of the interactions between SRC-1 and LXR/RXR heterodimers, FEBS Lett. 584 (2010) 3862–3866.

[21] R. Houtman, R. de Leeuw, M. Rondaij, D. Melchers, D. Verwoerd, R. Ruijtenbeek, J.W. Martens, J. Neefjes, R. Michalides, Serine-305 phosphorylation modulates estrogen receptor alpha binding to a coregulator peptide array, with potential application in predicting responses to tamoxifen, Mol. Cancer Ther. 11 (2012) 805–816.

[22] C.A. Flaveny, K. Griffett, B.E.M. El-Gendy, M. Kazantzis, M. Sengupta, A.L. Amelio, A. Chatterjee, J. Walker, L.A. Solt, T.M. Kamenecka, T.P. Burris, Broad anti-tumor activity of a small molecule that selectively targets the Warburg effect and lipogenesis, Cancer Cell 28 (2015) 1–15.

[23] A.S. Veleiro, A. Pecci, M.C. Monteserin, R. Baggio, M.T. Garland, C.P. Lantos, G. Burton, 6,19-Sulfur-bridged progesterone analogues with antiimmunosuppressive activity, J. Med. Chem. 48 (2005) 5675.

[24] A. Sali, T.L. Blundell, Comparative protein modelling by satisfaction of spatial restraints, J. Mol. Biol. 234 (1993) 779.

[25] M.J. Frisch, G. W. T, H.B. Schlegel, G.E. Scuseria, M.A. Robb, J.R. Cheeseman, J.A. Montgomery Jr., T. Vreven, K.N. Kudin, J.C. Burant, J.M. Millam, S.S. Iyengar, J. Tomasi, V. Barone, B. Mennucci, M. Cossi, G. Scalmani, N. Rega, G.A. Petersson, H. Nakatsuji, M. Hada, M. Ehara, K. Toyota, R. Fukuda, J. Hasegawa, M. Ishida, T. Nakajima, Y. Honda, O. Kitao, H. Nakai, M. Klene, X. Li, J.E. Knox, H.P. Hratchian, J.B. Cross, V. Bakken, C. Adamo, J. Jaramillo, R. Gomperts, R.E. Stratmann, O. Yazyev, A.J. Austin, R. Cammi, C. Pomelli, J.W. Ochterski, P.Y. Ayala, K. Morokuma, G.A. Voth, P. Salvador, J.J. Dannenberg, V.G. Zakrzewski, S. Dapprich, A.D. Daniels, M.C. Strain, O. Farkas, D.K. Malick, A.D. Rabuck, K. Raghavachari, J.B. Foresman, J.V. Ortiz, Q. Cui, A.G. Baboul, S. Clifford, J. Cioslowski, B.B. Stefanov, G. Liu, A. Liashenko, P. Piskorz, I. Komaromi, R.L. Martin, D.J. Fox, T. Keith, M.A. Al-Laham, C.Y. Peng, A. Nanayakkara, M. Challacombe, P.M.W. Gill, B. Johnson, W. Chen, M.W. Wong, C. Gonzalez, J.A. Pople, Gaussian, Inc., Wallingford CT, 2004.

[26] D.A. Case, T.E. Cheatham 3rd, C.L. Simmerling, J. Wang, R.E. Duke, R. Luo, R.C. Walker, W. Zhang, K.M. Merz, B. Roberts, S. Hayik, A. Roitberg, G. Seabra, J. Swails, A.W. Goetz, I. Kolossváry, K.F. Wong, F. Paesani, J. Vanicek, R.M. Wolf, J. Liu, X. Wu, S.R. Brozell, T. Steinbrecher, H. Gohlke, Q. Cai, X. Ye, J. Wang, M.-J. Hsieh, G. Cui, D.R. Roe, D.H. Mathews, M.G. Seetin, R. Salomon-Ferrer, C. Sagui, V. Babin, T. Luchko, S. Gusarov, A. Kovalenko, P.A. Kollman, Amber 12, 2012.

[27] T.E. Cheatham III, P. Cieplak, P.A. Kollman, A modified version of the Cornell et al. force field with improved sugar pucker phases and helical repeat, J. Biomol. Struct. Dyn. 16 (1999) 845.